

# Computational study of blood flow in lower extremities under intensive physical load

S. Simakov<sup>a1</sup>, T. Gamilov<sup>a</sup>, Y.N. Soe<sup>a</sup>

<sup>a</sup> Moscow Institute of Physics and Technology  
141700, Dolgoprudny, 9 Institutskii Lane, RUSSIA

## Аннотация

This work is aimed at computational study of blood flow in lower extremities under intensive physical load. We present a modified 1D cardiovascular system model describing skeletal-muscle pumping and autoregulation effects to the blood flow in lower extremities. Skeletal-muscle pump effect is introduced as an external time-periodical pressure function applied to a group of the veins. Period of this function is associated with the two strides period during running. Computational study reveals explicit optimal stride frequency providing maximum blood flow through the lower extremities. It is shown that optimal stride frequency depends on the personal parameters. The model is validated by comparison to the stride frequencies of a number of top level athletes therefore providing a method to assess the level of physical conditioning.

## 1 Introduction

The state of the art of modern cardiovascular system simulations includes 1D flow modeling in the network of elastic tubes [3, 6, 8, 15, 16] that is in some cases extended by 3D models for local regions resulting in fluid-structure interaction problem [6] and multidimensional 1D-3D coupling [5, 6]. The most works in this field consider normal or quiet state of the organism. The deeper look to the cardiovascular system simulation should include physiological reactions of the vessels wall [3, 9] and their interaction with surrounding tissues that is especially important for physical activity simulations.

This work is focused on mathematical model of cardiovascular system capable to simulate blood flow during physical load. We use 1D network dynamical model of global circulation [8, 16] taking only systemic circulation. This model is extended with the models of vascular autoregulation and skeletal-muscle pump including venous valves. Along with general pressure and velocity profile adjustments we validate this model by comparison of its response to

---

<sup>1</sup>Corresponding author. E-mail: simakov@crec.mipt.ru

the laboratory observations for the cases of gravitational and occlusion sampling tests and changing body's orientation in gravitational field.

We limited our discussion by periodic activity associated with low extremities muscles working. That is also can be associated with short-distance running. Mean blood flow in anterior tibial vein is mainly observed as a measure of low extremities muscles blood supply. Presented simulations reveal dependence of average blood flow and stride frequency during walking and running. As a result we observe particular value of stride frequency providing maximum average blood flow in anterior tibial vein that is associated with optimal stride frequency. This value is calculated and compared for several top level athletes. Good coincidence allows us to conclude that it could be a measure of sportsman effectiveness.

## 2 Methods

### 2.1 Systemic circulation

As a core model for blood circulation we used 1D network dynamical model [8, 16] taking into account systemic arteries and veins. The model is based on the model of viscous incompressible fluid flow through the network of elastic tubes. The flow in every vessel is described in terms of mass and momentum balance

$$\partial S_k / \partial t + \partial(S_k u_k) / \partial x = 0, \quad (2.1)$$

$$\partial u_k / \partial t + \partial(u_k^2 / 2 + p_k / \rho) / \partial x = f_{fr}(S_k, u_k, S_k^0) + g \sin \theta_k, \quad (2.2)$$

where  $k$  is an index of the vessel;  $t$  is time;  $x$  is distance along the vessel counted from the vessel's junction point;  $\rho$  is blood density (constant);  $S_k(t, x)$  is vessels's cross-section area;  $p_k$  is blood pressure;  $S_k^0$  is unstressed cross-sectional area;  $u_k(t, x)$  is linear velocity averaged over the cross-section;  $g$  is a gravity constant;  $\theta_k$  is an angle between the vessel and gravity field;  $f_{tr}$  is a friction force given by

$$f_{tr}(S_k, u_k, S_k^0) = -\frac{4\pi\mu u_k}{S_k^2} \left( \frac{S_k}{S_k^0} + \frac{S_k^0}{S_k} \right) \quad (2.3)$$

where  $\mu$  is blood viscosity.

In the statement of boundary conditions it must be taken into account that equations (2.1) and (2.2) are of a hyperbolic type. Boundary conditions for this type of equations shall be set, allowing for the behavior of characteristic curves on the border of the integration domain. Namely, at any moment of time within the period considered, the number of boundary conditions at each point of the boundary must correspond to the number of characteristic curves going out of the region at this point. Simultaneously, the conditions imposed by the equations of characteristic curves entering the domain (compatibility conditions) must be included. Therefore, it is essential to determine the behavior of the characteristic curves of equations (2.1) and (2.2). Denoting

$$\mathbf{V}_k = \{S_k, u_k\}, \quad \mathbf{F}_k = \{S_k u_k, u_k^2 / 2 + p_k / \rho\}, \quad \mathbf{g}_k = \{\phi_k, \psi_k\}$$

we write equations (2.1) and (2.2) in a divergence form:

$$\partial \mathbf{V}_k / \partial t + \partial \mathbf{F}_k / \partial x = \mathbf{g}_k.$$

Then, by the scalar multiplication by the left eigenvectors  $\boldsymbol{\omega}_{ki}$  ( $i = 1, 2$ ) of the Jacobi matrix  $\mathbf{A}_k = \partial \mathbf{F}_k / \partial \mathbf{V}_k$  we obtain the characteristic form of (2.1) and (2.2)

$$\boldsymbol{\omega}_{ki} \cdot (\partial \mathbf{V}_k / \partial t + \partial \mathbf{F}_k / \partial x) = \boldsymbol{\omega}_{ki} \cdot (\partial \mathbf{V}_k / \partial t + \lambda_{ki} \partial \mathbf{V}_k / \partial x) = \boldsymbol{\omega}_{ki} \cdot \mathbf{g}_k, \quad i = 1, 2 \quad (2.4)$$

where  $\lambda_{ki}$  are the eigenvalues of the matrix  $\mathbf{A}_k$ .

The specific expression for  $\mathbf{A}_k$ , by definition

$$\mathbf{A}_k = \partial \mathbf{F}_k / \partial \mathbf{V}_k = \begin{pmatrix} u_k & S_k \\ \frac{1}{\rho} \frac{\partial p_k}{\partial S_k} & u_k \end{pmatrix}.$$

Eigenvalues  $\lambda_{ki}$  can be found from

$$\det(\mathbf{A}_k - \lambda_k \mathbf{E}) = 0, \quad \mathbf{E} = \begin{pmatrix} 1 & 0 \\ 0 & 1 \end{pmatrix},$$

the solution of this equation is given by

$$\lambda_{ki} = u_k + (-1)^i \sqrt{\frac{S_k}{\rho} \frac{\partial p_k}{\partial S_k}}, \quad i = 1, 2. \quad (2.5)$$

Left eigenvectors  $\boldsymbol{\omega}_{ki}$  are determined from equations (except for constant factor)

$$\boldsymbol{\omega}_{ki} (\mathbf{A}_k - \lambda_{ki} \mathbf{E}) = 0, \quad i = 1, 2$$

and it is possible to choose, for example

$$\boldsymbol{\omega}_{ki} = \left\{ \sqrt{\frac{1}{\rho} \frac{\partial p_k}{\partial S_k}}, (-1)^i \right\}, \quad i = 1, 2. \quad (2.6)$$

The value  $\sqrt{\frac{S_k}{\rho} \frac{\partial p_k}{\partial S_k}}$  from (2.5) is the velocity of small disturbances. In all parts of the cardiovascular system during the normal functioning and in cases of most pathologies velocity of small disturbances is bigger than blood flow velocity  $u_k$ . For such flows, as follows from (2.5), in each point of the considered domain at any moment of time, one of the characteristic curves has a positive slope and the other has a negative slope. In the statement of boundary conditions, therefore, only one condition should be set at the inlet and outlet of the elastic tube.

At the entry point of the vessel connected to the heart the blood flow is assigned as the boundary condition

$$u(t, 0) S(t, 0) = Q_H(t). \quad (2.7)$$

At the terminal point of the venous system ( $x = x_H$ ) the pressure is set as the boundary condition

$$p_H(t, x_H) = p_H. \quad (2.8)$$

At the vessels junctions the Poiseulle's pressure drop condition and the mass conservation condition are stated

$$p_k(S_k(t, \tilde{x}_k)) - p_{node}^l(t) = \varepsilon_k R_k^l S_k(t, \tilde{x}_k) u_k(t, \tilde{x}_k), k = k_1, k_2, \dots, k_M, \quad (2.9)$$

$$\sum_{k=k_1, k_2, \dots, k_M} \varepsilon_k Q_k(t, \tilde{x}_k) = 0, \quad (2.10)$$

where  $M$  is number of the connected vessels,  $\{k_1, \dots, k_M\}$  is range of the indices of the connected vessels,  $p_{node}(t)$  is pressure at the junction point,  $\varepsilon = 1, \tilde{x}_k = 0$  for incoming vessels,  $\varepsilon = -1, \tilde{x}_k = L_k$  for outgoing vessels.

Every boundary condition (2.7)–(2.10) is extended with compatibility condition of the hyperbolic set (2.1), (2.2). After finite differences discretization it provides linear dependence between linear velocity  $u_k(t_{n+1}, \tilde{x}_k)$  and cross section area  $S_k(t_{n+1}, \tilde{x}_k)$  at the upper time layer at the end or at the beginning of every vessel composing a node

$$u_k(t_{n+1}, \tilde{x}_k) = \alpha_k S_k(t_{n+1}, \tilde{x}_k) + \beta_k. \quad (2.11)$$

The nonlinear set (2.9)–(2.11) of  $2M + 1$  equations can be reduced to the set of  $M$  equations [4] and can be effectively solved by Newton method.

Coefficients  $\alpha$  and  $\beta$  for (2.11) can be derived using finite differences discretization of (2.4) (index  $k$  is suppressed but implicitly assumed until the end of this section). For each vessel we use uniform 1D mesh

$$M = \{(x_j, t_n) : x_j = hj, hJ = L, j = \overline{0, J}; t_n = \sum_{p=1}^n \tau_p\}$$

where  $h$  is spatial step,  $\tau_p$  is a  $p$ -th time step. For the beginning of the vessel outgoing from the node we looking for  $\mathbf{V}(0, t_{n+1})$  taking  $\mathbf{V}(0, t_n)$  from the previous time step and  $\mathbf{V}(x_1, t_{n+1})$  from the internal points explicit computational algorithm [4]. Taking

$$\left(\frac{\partial \mathbf{V}}{\partial x}\right)_{0, t_{n+1}} \approx \frac{\mathbf{V}(x_1, t_{n+1}) - \mathbf{V}(0, t_{n+1})}{h}, \quad \left(\frac{\partial \mathbf{V}}{\partial t}\right)_{0, t_{n+1}} \approx \frac{\mathbf{V}(0, t_{n+1}) - \mathbf{V}(0, t_n)}{\tau_{n+1}},$$

$$(\boldsymbol{\omega}_i)_{0, t_{n+1}} \approx (\boldsymbol{\omega}_i)_{0, t_n}, \quad (\lambda_i)_{0, t_{n+1}} \approx (\lambda_i)_{0, t_n},$$

and denoting  $w = \sqrt{\frac{1}{\rho} \left(\frac{\partial p}{\partial S}\right)_{0, t_n}}$ ,  $\mathbf{W} = \{w, (-1)^i\}$ ,  $\sigma = \frac{\tau_{n+1}}{h} (\lambda_i)_{0, t_n}$  we can discretize (2.4) for the inlet ( $i = 1$ ) as

$$\mathbf{W} \cdot \left( \frac{\mathbf{V}(0, t_{n+1}) - \mathbf{V}(0, t_n)}{\tau_{n+1}} + (\lambda_i)_{0, t_n} \frac{\mathbf{V}(x_1, t_{n+1}) - \mathbf{V}(0, t_{n+1})}{h} \right) = \mathbf{W} \cdot \mathbf{g}. \quad (2.12)$$

That can be rewritten in the form (2.11) taking

$$\alpha = w, \beta = \frac{w(\sigma S(x_1, t_{n+1}) - S(0, t_n)) + u(0, t_n) - \sigma u(x_1, t_{n+1}) - \tau_{n+1}(w\phi - \psi)}{1 - \sigma}.$$

The same method applied to the outlet conditions results in

$$\alpha = -w, \beta = \frac{w(\sigma S(x_{J-1}, t_{n+1}) + S(x_J, t_n)) + u(x_J, t_n) + \sigma u(x_{J-1}, t_{n+1}) + \tau(w\phi + \psi)}{1 + \sigma}.$$

## 2.2 Wall-state equation

Elastic properties of the vessel wall material are described by the wall-state equation providing response to the transmural pressure (the difference between blood pressure and pressure in the tissues surrounding the vessel)

$$p_k(S_k) - p_{*k} = \rho c_k^2 f(S_k), \quad (2.13)$$

where S-like function  $f(S)$  is approximated as

$$f(S_k) = \begin{cases} \exp(S_k/S_k^0 - 1) - 1, & S_k > S_k^0 \\ \ln(S_k/S_k^0), & S_k \leq S_k^0 \end{cases}, \quad (2.14)$$

$p_{*k}$  is pressure in the tissues surrounding the vessel,  $c_k$  is small disturbances propagation velocity of the wall material in the relaxed state ( $S_k = S_k^0$ ) which can be interpreted as pulse wave velocity (PWV) in the unstressed vessel [19].

As is shown in section 3 the purely mechanical model presented in this section fails to describe correctly some of the features related to the transient states, e.g. changing body orientation in gravity field, vessels occlusion and others. Real vascular networks include regulatory and venous blood return mechanisms (muscle pump, venous valves, respiratory pump and others [14]) that can substantially affect pressure and velocity profiles. Some of this effects are introduced in the following section.

## 2.3 Autoregulation

We consider blood flow autoregulation as response of the arteries wall elasticity to changes in averaged blood parameters (such as mean pressure, mean blood flow, oxygen concentration). Laboratory study presented at Figure 1 reveals vessel's initial expanding (passive phase) and subsequent gradual contraction (active phase) under induced blood pressure increase. It results in maintaining constant mean blood flow despite changes in pressure.

Autoregulation is a local effect occurred even in isolated blood vessels. According to [7] there are many potentially important mechanism of autoregulation - myogenic, metabolic, tissue pressure et. al. Each mechanism has its own experimental evidence. We use only myogenic hypothesis in this work as it has straightforward mechanical interpretation and probably plays the dominant role for intensive physical loads considered in this work.

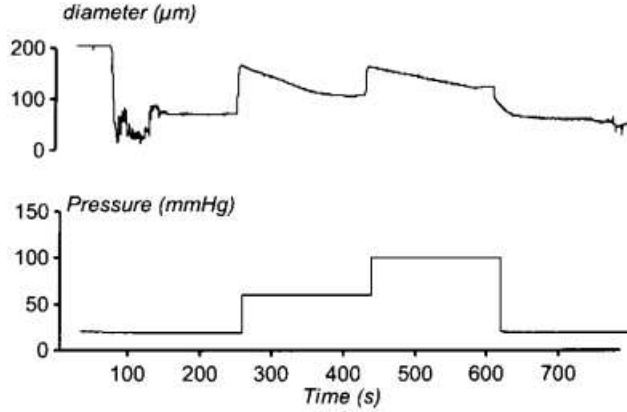


Рис. 1: The effect of subsequent pressure steps on diameter of rat artery [1]

According to myogenic hypothesis vascular smooth muscle responds to the changes of the mean pressure. The mean pressure increase results in the vascular smooth muscle contraction which results in the vessel's stiffness increase consequently providing higher pulse wave velocity. The same is valid for the mean pressure decrease resulting in vascular smooth muscle relaxation and decrease both the stiffness and pulse wave velocity.

Vascular smooth muscle cells responded to the mean pressure changes are placed in tunica media (the middle layer of a blood vessel wall). This layer is quite thick in arteries and relatively thin in veins. As a result myogenic autoregulation in veins provides no substantial impact to the blood flow and we remove it from consideration.

These observations may be incorporated to our model as follows. Cross-section area  $S_k$  and blood pressure  $p_k$  are related by parameter  $c_k$ . Supposing cross-section area to be constant and applying (2.13) to it we will derive the following dimensionless time-independent parameter

$$\frac{\bar{p}_k - \bar{p}_{*k}}{\rho c_k^2} = \overline{f(S_k)} = const. \quad (2.15)$$

It requires computational algorithm modification. Autoregulation is not an instant process. To avoid significant changes in vessels properties during a single heart period we should take an average of (2.15) over time. Assuming  $\bar{p}_{*k} = 0$  in arteries and  $\rho = const$

$$\frac{\bar{p}_k}{c_k^2} = const. \quad (2.16)$$

Taking average pressure during two subsequent averaging periods  $T_1, T_2$  throughout the vessel  $k$  we can recalculate new value  $c_k$  for the next period  $T_3$  and so on

$$\frac{c_{k,new}}{c_{k,old}} = \sqrt{\frac{\bar{p}_{k2}}{\bar{p}_{k1}}}, \quad (2.17)$$

where  $\bar{p}_{kj}$  is average transmural pressure for the averaging period  $T_j$ . The smallest averaging period should be greater or equal to the heart period as mean pressure may substantially change during smaller periods. We use 4 seconds for all averaging periods as it provides more stable solution in our numerical experiments. This value is substantially smaller than characteristic time of the simulations that is 100 – 200 seconds.

## 2.4 Skeletal-muscle pump

In this work we consider physical load specific for running. It is characterized by periodic activity of the muscles of the low extremities. Due to anatomical feature skeletal-muscle pump does not affect large arteries [14] and we remove them from the further consideration. Assuming the force compressing the vein to be directed perpendicularly to its axis allows to relate muscle pumping with external pressure  $p_{*k}$  in (2.13). Maximum value of this pressure may be derived if we consider muscle as a cylinder holding the weight of a human body which gives us [11]

$$p_{*k} = \frac{mg}{S} \frac{\sigma}{1 - \sigma} \quad (2.18)$$

where  $m$  is a mass of the body;  $S$  is muscle average cross-section;  $\sigma$  is muscle's Poisson ratio. Taking for a trained athlete  $m = 60kg$ ,  $\sigma = 0.49$  and  $S = 600cm^2$  we evaluate  $p_{*k}$  as  $10kPa$ .

We consider running as periodical processes with period  $T$ . This period is equal to the time needed for two complete strides. Thus the stride frequency is

$$\nu = \frac{2}{T}. \quad (2.19)$$

As a result muscle-pumping pressure can be given by

$$p_{*k} = \frac{P_{max}}{2} \left( 1 + \sin \left( \frac{2\pi t}{T} + \Phi \right) \right) \quad (2.20)$$

where  $P_{max} = 10kPa$ ,  $\Phi$ — phase ( $\Phi_l = 0$  for the left leg and  $\Phi_r = \frac{\pi}{2}$  for the right).

Additional feature of the major leg's veins substantial for the muscle-pumping is the valves functioning preventing the backward blood flow [14]. The mechanism of the valves functioning is shown on Figure 2 .

We propose to simulate this feature by modifying friction force (2.3) as

$$F_{fr} = \begin{cases} f_{fr}(s, u), & u > 0 \\ A, & u < 0 \end{cases} \quad (2.21)$$

where  $f_{fr}(s, u)$  is a friction force used in general non-valved vessel (2.3),  $A \gg f_{fr}$  (in this work  $A = 100f_{fr}$ ) is a virtual force used to prevent the backward flow. It of course differs from the actual venous valves functioning. Here we implicitly assume instant venous valves activation immediately after the linear velocity comes below zero. For the real case small time-lag is observed and some relatively small negative value of the linear velocity may achieved. We neglect this kinetic energy losses especially within the scope of short time simulations carried in this work.

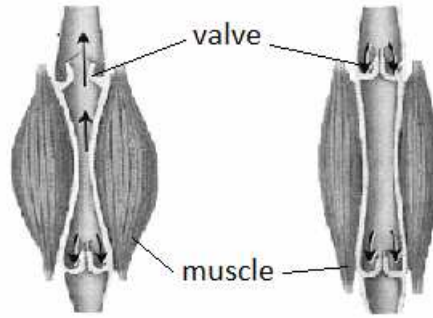


Рис. 2: Venous valves.

## 2.5 Integration domain and model identification

We suppose that the networks of the arteries and veins have the same structure. Corresponding vessels have the same length ( $L_k^{art} = L_k^{ven}$ ), diameters of the corresponding veins two times greater than that for the arteries ( $d_k^{art} = 2d_k^{ven}$ ). The total network of systemic circulation is composed by joining arterial and venous network by virtual vessels having averaged properties corresponding to the peripheral circulation. Parameters of these terminal vessels were specified so as they contain about 20% of the total blood volume and provide adequate pressure and blood velocity difference between arteries and veins according to [14]. General scheme of the network is shown at Figure 3. Structural and functional parameters of the network were specified according to the available data [14, 17, 15]. More detailed description on the methods of integration domain and model identification can be found in [8, 16].

Specific case considered in this work relates to the cardiovascular simulation under intensive physical load. This is generally applicable to the sportsmen and other specially trained persons. We use PWV index to specify vessel's wall elasticity more adequate as trained athletes are characterized by increased elasticity and consequently lower PWV values [12, 13]. The vascular network was also fitted by the body's height by appropriate scaling of the vessel's lengths.

## 3 Results

Developed model was identified, tested and validated by different methods described in [8, 16]. Most similar related works provide pressure, linear velocity or blood flow profile adjustment to some laboratory or generally known in physiology data. This of course confirms the models. For the case of physical activity simulations when autoregulation plays important role it is also important to adjust the model response to some static and dynamical disturbances. In the beginning of this section we validate our model by comparison of its response to the laboratory observations for the cases of gravitational and occlusion sampling tests and changing body's orientation in gravitational field. The rest of the section presents results of

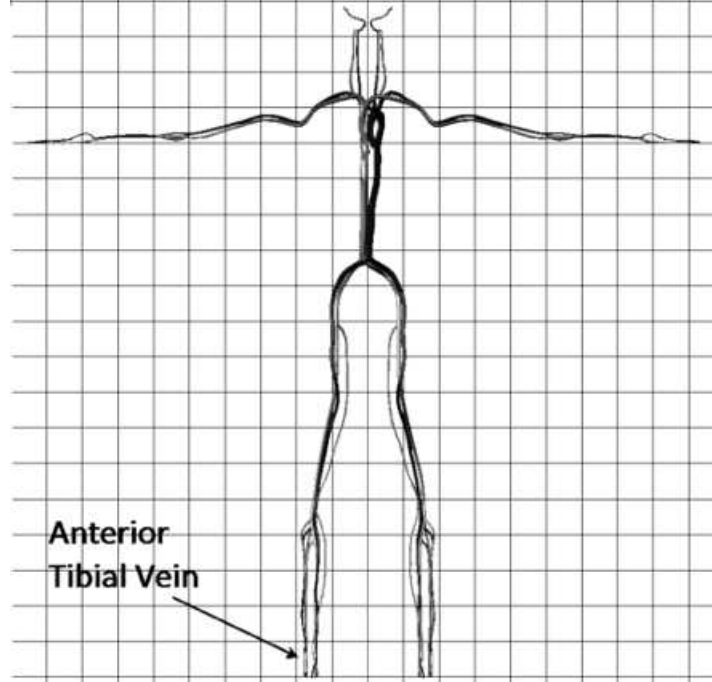


Рис. 3: The scheme of arterial and venous vessel networks.

the computational study of blood flow in lower extremities under intensive physical load.

### 3.1 Model validation

The scheme of the gravitational sampling is presented at Figure 4. Arterial volume distensibility was experimentally measured in [20] from the electrocardiogram and finger and ear photoplethysmograms records from 15 subjects with the right arm at five different positions ( $90^\circ$ ,  $45^\circ$ ,  $0^\circ$ ,  $-45^\circ$  and  $-90^\circ$  degrees referred to the horizontal level). By definition, arterial volume distensibility  $D_v$  gives relative blood volume change in selected vascular region with a known change in arterial pressure

$$D_v = \frac{1}{\Delta P} \frac{\Delta V}{V}$$

According to [20] it can be rewritten as

$$D_v = \frac{1}{\rho a^2} \quad (3.1)$$

where  $a$  is a pulse wave velocity. (3.1) is used for validation of the model presented in this work.

Experimental series described in [20] were simulated by our model. Results of numerical simulations are presented on Figure 5 along with the data from [20]. It allows to conclude that they are in quite good qualitative and even quantitative agreement.

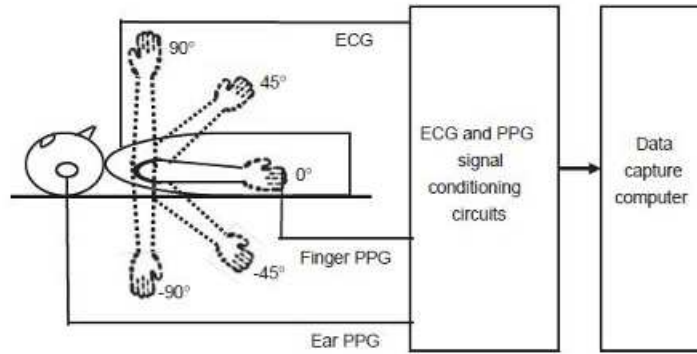


Рис. 4: The scheme of the experiment [20].

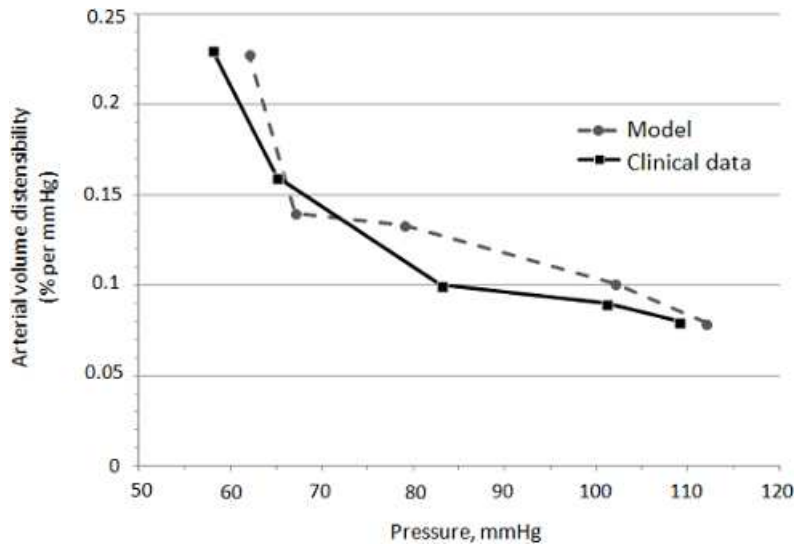


Рис. 5: Relationship between mean arterial pressure and arterial volume distensibility

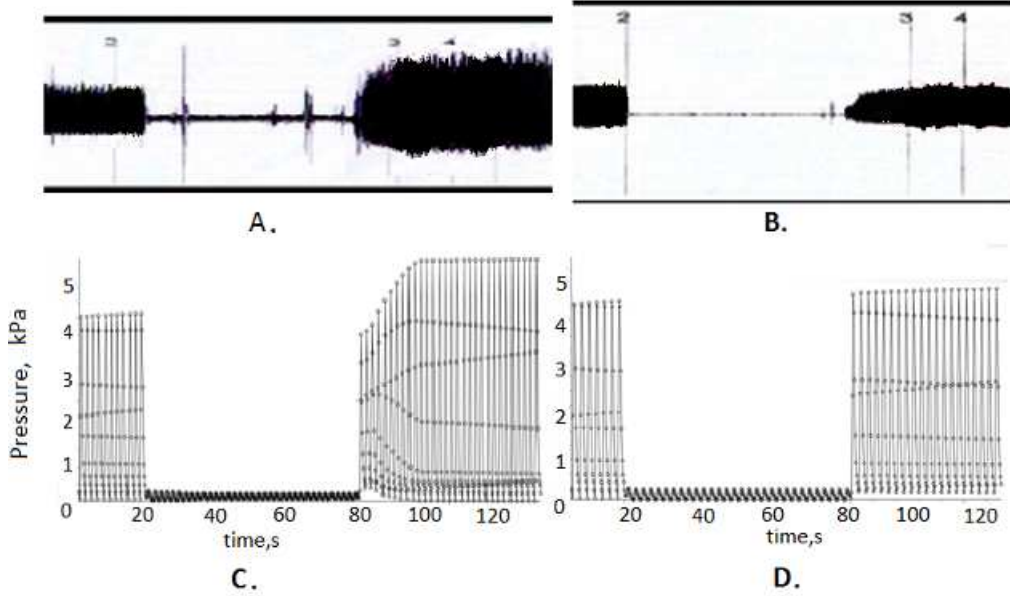


Рис. 6: A and B — PAT signals (measured from a finger) during cuff occlusion [10]. for healthy and diseased subjects. C and D — numerically calculated pressure in a finger during occlusion with and without autoregulation.

Occlusion sampling test is described in [10]. It involves measuring Peripheral Arterial Tone (PAT) signal from a finger during brachial artery occlusion. Healthy subjects show increased PAT signal during recovery which corresponds to the average blood pressure increase in peripheral arteries while unhealthy subjects with inadequate autoregulation show blunted response. The results of numerical simulation of this test are shown on Figure 6. We only mention qualitative coincidence here as available analog PAT signal is not directly recalculated to pressure. In most cases higher average pressure leads to the higher arterial tone and PAT amplitude but it can be invalid for some specific cases, such as obstructive sleep apnea [18].

Next dynamical test of our model is based on the simulation of the body orientation in gravitational field. It is known that body position change from horizontal to vertical causes the blood pressure increase e.g. in anterior tibial artery. Cross-section initially increases and then returns towards normal level due to autoregulation effect. In this simulation we consider vascular network to be at rest for the first 80 seconds. After that gravitational impact is activated by the right part of (2.2). We assume it corresponding to change in body position from horizontal to vertical. Calculated anterior tibial artery cross-sections with the time are depicted at Figure 7. Qualitatively the model's behavior corresponds to the loaded rat arteries behavior [1] presented at Figure 1.

Figure 7 shows that the model with autoregulation is capable to provide correct response to some external disturbances such as body position change. After standing up leg arteries

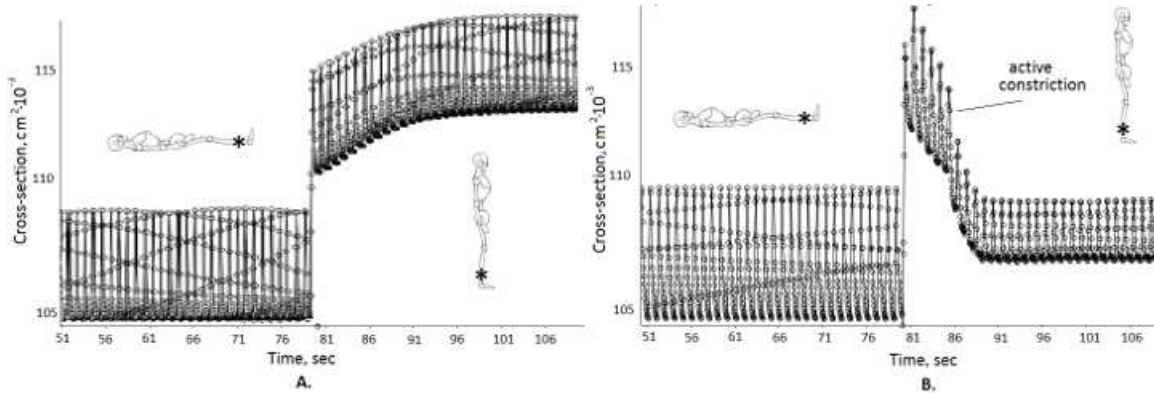


Рис. 7: The effect of changing body position on cross-section of anterior tibial artery without (A) and with (B) autoregulation.

contracted to neutralize blood pressure increase in lower extremities. Excessive blood pressure in the lower body could lead to increased load on venous valves resulting in their malfunctioning. This in turn is the reason for such vascular disease as varicose veins etc. The other important physiological reason for maintaining blood pressure in the lower body at the same level as before standing is to neutralize sudden pressure drop in brain. Sudden pressure drop in upper body could be the reason for orthostatic hypotension [2] such as dizziness, blurred or dimmed vision or even faint. It is especially important for adults commonly experiencing regulatory mechanisms malfunctions.

### 3.2 Skeletal-muscle pump

Developed model allows us to simulate blood flow in the legs during intensive exercise taking into account specific vessels elasticity of the trained athletes and their height. In each simulation we consider the vascular network to be at rest for the first 90 seconds to assure pseudo steady pulsate state maintained all over the network. After that an external pressure (2.20) is applied to the leg veins for the next 70 seconds. Mainly anterior tibial vein (Figure 3) was observed. The blood flow was averaged over the 4 cardiac cycles. The results of the first series include simulations of the mean blood flow in tibial vein for different stride frequencies (Figure 8). From Figure 8 one can observe an increase of the blood flow along with the stride frequency increase until some optimal value is achieved. The further increase of the stride frequency results in the blood flow decrease. We address to this value as to the optimal stride frequency as it provides maximum blood supply consequently resulting in maximum muscles oxygen supply due to convective transport by blood.

The next computational series showed that optimal stride frequency depends on the total length of the vessels' network and elastic properties of the vessels' walls and does not depend on boundary conditions on heart. In the simulations presented in this work elastic properties were set according to PWV data for trained athletes [12, 13]. Figure 8 demonstrates stride

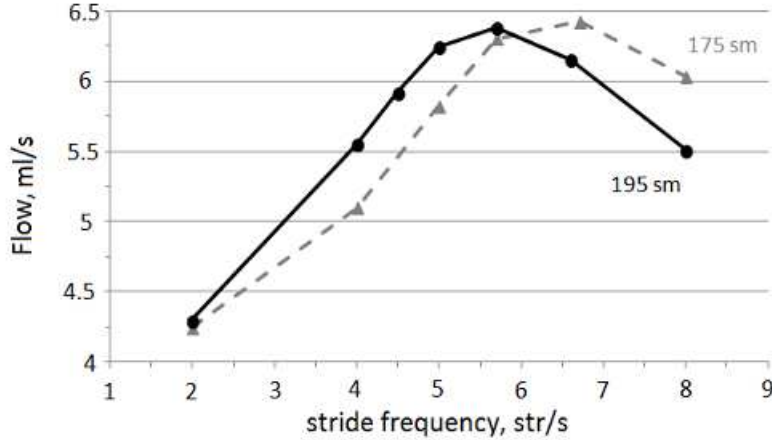


Рис. 8: Stride frequency for the networks fitted to the body's height of 175 cm and 195 cm.

	A	B	C	D
Height, cm	195	175	183	124
Stride frequency, str/sec	$4.27 \pm 0.05$	$4.7 \pm 0.1$	$4.54 \pm 0.02$	$6.40 \pm 0.05$

Таблица 1: Actual parameters of the athletes. A, B, C, D notations are presented in the text

frequency dependence from the body's height. In this simulations vessels lengths were fitted to the height by linear scaling

$$L_{k2} = \frac{H_2}{H_1} L_{k1}, \quad (3.2)$$

where  $H_{1,2}$  is height of the body in two simulations,  $L_{k1,2}$  is length of the k-th vessel in two simulations.

More detailed computational analysis is presented on Figure 9. Optimal stride frequency is simulated for several selected heights. It is compared to several well-known results in the recent world level competitions. We selected gold (A) and bronze (B) medal winners in 100 meters sprint in Beijing 2008 Olympiad, bronze medal winner in 100 meters sprint in London 2012 Olympiad (C) and gold medal winner in 100 meters sprint in World Dwarf Games 2008 (D). Actual sportsmen stride frequency and height was measured from the free online video available in the World Wide Web. These parameters are summarized in the Table 1.

From Figure 9 one can observe quite good agreement between simulated and actual optimal stride frequencies in the wide range of the heights. We should mention that the model used for these simulations provides rather qualitative than quantitative description. It includes some physiological effects such as muscular pumping with venous valves and myogenic autoregulation mechanism. But many other important effects such as metabolic and tissue pressure autoregulation mechanisms, other regulatory systems, heart rate variability, oxygen transport, respiratory system, energy production and supply by the organism and

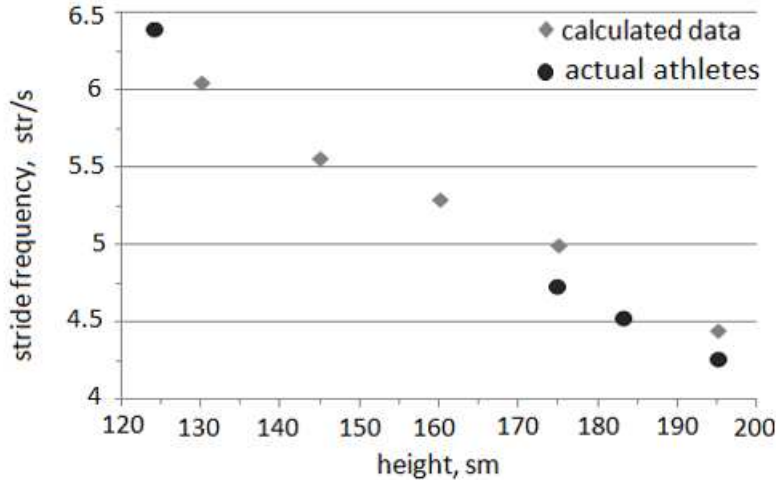


Рис. 9: Optimal stride frequency for trained athletes.

others are not included. Nevertheless computed values are very close to the actual data (Figure 9). It provides evidence for valid blood flow simulating under intensive physical load within the proposed approach. The further simulations are needed to validate this model which should include more different athletes specializing in long-distance running as well.

## 4 Discussion

It should be pointed out that presented numerical experiments on computing optimal stride frequency consider blood flow optimization for sprinters. But the period of 70 seconds selected for calculating optimal stride frequency is far beyond the actual time needed to finish 100 meters distance which is less than 10 seconds. The model application is also limited by the fact that 4 seconds period is selected for averaging mean blood pressure for the next stage controlled by autoregulation response of again 4 seconds. It also should be mentioned that blood supply plays minor role for short-distance runners as major energy is anaerobically produced by tissues. So if sprint is considered there is no direct analogy with real competition even if actual parameters are set for simulations. In addition computational domain structure used in this work is quite far from the real vascular network as only major arteries and veins included and only systemic circulation is considered.

Inlet and outlet boundary conditions (2.7)–(2.8) to the vascular network corresponding to the heart junctions can't guarantee mass conservation in the system in general. Nevertheless a wide range of the previously performed simulations revealed good quantitative coincidence in the quiet state of the system [4, 8, 16]. In the case of the intensive physical load such approach produces more error. Along with the other assumptions such as constant heart rate and absence of the baroreflex regulation it will be one of the central questions of the

future work. We just used this simplified approach for very limited time domain (less than 70 seconds). Thus the model sensibility to these effects is negligible. We also conclude that the flow maximum at optimal stride frequency is mostly related to the local elastic properties of the region of the lower extremities.

We can assume that professional sprinters have stride frequencies that are very close to the optimal ones. It might be due to a natural born talent or years of hard work. It is possible to adjust vessels' elastic properties via combining endurance- and strength-based exercises. It looks like elite sprinters trained their circulatory system (involuntarily) in a way that their optimal frequency and stride frequency are very close.

Nevertheless it seems that optimal stride frequency computed by our method strongly correlates with observations. It seems to be a possible measure of sportsman effectiveness as far as ordinary organism simulations provide greater deviations from this value. Such simulations can't be presented in systemic way due to substantial variability for not trained persons. Moreover it may provide more realistic criterion if other sport events with periodical physical load and longer time periods would be considered. This is a starting point for further development of this work.

This work was partially supported by the grants RFBR 11-01-00855-a, 11-01-00971 and MK 2719.2012.9.

## Список литературы

- [1] E.VanBavel, J.P.Wesselman, J.A.Spaan, Myogenic Activation and Calcium Sensitivity of Cannulated Rat Mesenteric Small Arteries, *Circ Res* 82, pp 210–220 (1998)
- [2] J.G. Bradley, K.A. Davis, Orthostatic Hypotension, *Am Fam Physician* 68, No 12, pp 2393–2399 (2003)
- [3] A. Ya. Bunicheva, M.A. Menyailova, S. I. Mukhin, N. V. Sosnin, , A. P. Favorskii, Investigation of Influence of Gravitational Overloads on Parameters of Blood Flow in the Systemic Circulation, *Matem Mod* 24, pp 67–82 (2012) (In Russian)
- [4] Yu. Vassilevski, S. Simakov, V. Salamatova, Yu. Ivanov, T. Dobroserdova, Numerical issues of modelling blood flow in networks of vessels with pathologies, *Russ J Numer Anal M* 26(6), pp 605–622 (2012)
- [5] T.K. Dobroserdova, M.A. Olshanskii, A finite element solver and energy stable coupling for 3D and 1D fluid models, *Comp Meth Appl Mech Eng* 259, pp 166-176 (2013)
- [6] L. Formaggia, A. Quarteroni, A. Veneziani, *Cardiovascular mathematics*, DE: Springer, Heidelberg, p.522 (2009)
- [7] P.C. Johnson, Autoregulation of blood flow, *Circ Res* 59, pp 482–495 (1986)
- [8] A.S. Kholodov, Some Dynamical Models of External Breathing and Blood Circulation Regarding to Their Interaction and Substances Transfer, in: *Comp. Mod. and Med. Prog., Science ,Moscow*, pp 127–163 (2001)

- [9] N.Kudryashov, I.Chernyavskii, Numerical Simulation of the Process of Autoregulation of the Arterial Blood Flow, *Fluid Dynamics* 43, p 32 (2008)
- [10] J. T Kuvin, A.R. Patel, K.A. Sliney, N.G. Pandian, J. Sheffy, R.P.Schnall, R.H.Karas, J.E.Udelson, Assessment of peripheral vascular endothelial function with finger arterial pulse wave amplitude, *Am Heart J* 146, pp 168–174 (2003)
- [11] L.D. Landay, E.M. Lifshitz, *Theory of Elasticity*, 3rd ed., Elsevier, Oxford, 1986
- [12] T. Otsuki, S. Maeda, M. Iemitsu, Y. Saito, Y. Tanimura, R. Ajisaka, T. Miyauchi, Relationship Between Arterial Stiffness and Athletic Training Programs in Young Adult Men, *Am J Hypertens* 146, pp 168–174 (2003)
- [13] R. Sala, C. Rossel, P. Encinas, P. Lahiguera, Continuum of Pulse Wave Velocity from Young Elite Athletes to Uncontrolled Older Patients with Resistant Hypertension, *J. Hypertens* 28, pp 19.216 (2010)
- [14] R.F. Schmidt, G. Thews, *Human Physiology*, vol.2, 2nd ed., MIR, Moscow, 1996 (In Russian)
- [15] S.J.Sherwin, L.Formaggia, J.Peiro, V.Franke, Computational modelling of 1D blood flow with variable mechanical properties and its application to the simulation of wave propagation in the human arterial system, *Int. J. Numer. Meth. Fluids* 43, No 6-7, pp 673–700 (2003)
- [16] S.S. Simakov, A.S. Kholodov, Computational Study of Oxygen Concentration in Human Blood under Low Frequency Disturbances, *Math. Mod. Comp. Sim* 1(2), pp 283–295 (2009)
- [17] S. Standring, *Gray’s Anatomy: The Anatomical Basis of Clinical Practice* 40th ed., Elsevier, Churchill-Livingstone, 2008
- [18] D. P. White Monitoring Peripheral Arterial Tone (PAT) to Diagnose Sleep Apnea in the Home, *J Clin Sleep Med* 4(1), Suppl.3, p 73, (2008)
- [19] I. B. Wilkinson, J. R. Cockcroft, D. J. Webb, Pulse wave analysis and arterial stiffness, *J. Cardiovasc. Pharmacol.* 32, Suppl.3, S33–7, (1998)
- [20] D.Zheng, A. Murray, Non-invasive quantification of peripheral arterial volume distensibility and its non-linear relationship with arterial pressure *J. Biomech* 42, pp 1032–1037 (2009)